

SCIENTIFIC REPORTS



OPEN

Highly Flexible Self-Assembled V_2O_5 Cathodes Enabled by Conducting Diblock Copolymers

Hyosung An¹, Jared Mike¹, Kendall A. Smith², Lisa Swank², Yen-Hao Lin², Stacy L. Pesek², Rafael Verduzco^{2,3} & Jodie L. Lutkenhaus¹

Received: 22 April 2015

Accepted: 18 August 2015

Published: 22 September 2015

Mechanically robust battery electrodes are desired for applications in wearable devices, flexible displays, and structural energy and power. In this regard, the challenge is to balance mechanical and electrochemical properties in materials that are inherently brittle. Here, we demonstrate a unique water-based self-assembly approach that incorporates a diblock copolymer bearing electron- and ion-conducting blocks, poly(3-hexylthiophene)-*block*-poly(ethyleneoxide) (P3HT-*b*-PEO), with V_2O_5 to form a flexible, tough, carbon-free hybrid battery cathode. V_2O_5 is a promising lithium intercalation material, but it remains limited by its poor conductivity and mechanical properties. Our approach leads to a unique electrode structure consisting of interlocking V_2O_5 layers glued together with micellar aggregates of P3HT-*b*-PEO, which results in robust mechanical properties, far exceeding the those obtained from conventional fluoropolymer binders. Only 5 wt % polymer is required to triple the flexibility of V_2O_5 , and electrodes comprised of 10 wt % polymer have unusually high toughness (293 kJ/m³) and specific energy (530 Wh/kg), both higher than reduced graphene oxide paper electrodes. Furthermore, addition of P3HT-*b*-PEO enhances lithium-ion diffusion, eliminates cracking during cycling, and boosts cyclability relative to V_2O_5 alone. These results highlight the importance of tradeoffs between mechanical and electrochemical performance, where polymer content can be used to tune both aspects.

There is a growing need for low-cost, flexible, and rugged energy storage devices compatible with emerging flexible energy conversion devices and structural energy and power^{1–4}. Recent work has demonstrated electrode materials with both mechanical robustness and electrochemical functionality, including carbon nanotube Bucky paper^{5–8}, reduced graphene oxide paper^{9–11}, graphite on super-aligned CNTs¹², TiO₂ on activated carbon fabric¹², and vanadium pentoxide (V_2O_5) wires¹³. Of these, V_2O_5 is particularly promising because it offers higher specific energy and because it has the ability to form paper-like electrodes very similar to Bucky paper. Unfortunately, the application of V_2O_5 in practical batteries has been hindered by a low Li⁺-diffusion coefficient (10^{–12}–10^{–13} cm²/s)¹⁴, low electronic conductivity (10^{–2}–10^{–3} S/cm)¹⁴ and volumetric changes¹⁵ during cycling.

Past approaches sought to address the electrochemical limitations of V_2O_5 by incorporation of conductive polymers, but little has been achieved by way of mechanical enhancement. Conjugated polymers can improve the electronic conductivity of V_2O_5 electrodes^{16,17}, and ethylene oxide-containing polymers have demonstrated improved ionic conductivity¹⁸. Besides the materials themselves, the manner in which the blend is prepared can have a huge impact on electrode structure and mechanical properties. Large-scale phase separation between different components can result in poor mechanical properties, so intimate mixing and good interfacial adhesion is important.

¹Artie McFerrin Department of Chemical Engineering, Texas A&M University, College Station, TX. ²Department of Chemical and Biomolecular Engineering, Rice University, Houston, TX. ³Department of Materials Science and NanoEngineering, Rice University, Houston, TX. Correspondence and requests for materials should be addressed to J.L.L. (email: rafaelv@rice.edu) or R.V. (email: jodie.lutkenhaus@tamu.edu)

To demonstrate a viable route to mechanically robust V_2O_5 electrodes, we propose the implementation of block copolymers, in which two polymers are covalently attached to each other preventing macroscopic phase separation¹⁹. There exist only a handful of studies that incorporate block copolymers into hybrid electrodes, highlighting that the largest challenge for these hybrid electrodes is to balance the benefits of the added conductivity from the polymer without diluting the active material. For instance, the Balsara group reported the use of poly(3-hexylthiophene)-*block*-poly(ethyleneoxide) P3HT-*b*-PEO block copolymer as a conductive binder for a $LiFePO_4$ cathode^{20,21}. $LiFePO_4$ performed at near-theoretical capacity, but a block copolymer loading of 50 wt% was required; mechanical properties were not reported. The Mayes group reported the synthesis of V_2O_5 aerogel within a block copolymer matrix¹⁸. This resulted in significantly improved mechanical properties, but the V_2O_5 content was only 34 wt%, resulting in a very low capacity. In both of these approaches, the loading of the active material was prohibitively low.

Here, our approach centers on a V_2O_5 hybrid electrode, in which we balance a high active material content with the benefits afforded by the P3HT-*b*-PEO block copolymer. The electrodes are prepared in a straightforward and scalable water-based process, and the addition of just 5 wt % block copolymer produces electrodes with excellent mechanical flexibility. We present the electrochemical and mechanical properties of the hybrid electrodes as a function of composition, for which a trade-off between polymer content and electromechanical properties is revealed. Specifically, we demonstrate that small amounts of a (P3HT-*b*-PEO) block copolymer can bring about significant improvements in mechanical flexibility, toughness, and lithium ion diffusion. The enhanced mechanical properties are attributed to the self-assembled layering of V_2O_5 with P3HT-*b*-PEO micellar aggregates. A proof-of-concept flexible half-cell is also shown. These results confirm that these ion- and electron-conducting block copolymers are excellent binders, bringing about not only conductivity but also mechanical flexibility.

Results and Discussion

Our approach to flexible hybrid battery electrodes was to combine P3HT-*b*-PEO block copolymer with V_2O_5 . The block copolymer contains electron- and ion-conducting P3HT and PEO blocks, respectively, whereas V_2O_5 has a high capacity for lithium ions. The challenge is to combine the two materials in such a manner so as to leverage the conductivity and flexibility of the polymer without compromising the electroactivity of the V_2O_5 . Thus processing and blending were key considerations.

P3HT-*b*-PEO was synthesized using a modified approach based upon our prior publication²². Briefly, reactive, end-functionalized P3HT and PEO macroreagents were synthesized separately and coupled through a copper-catalyzed azide-alkyne click coupling reaction (see Scheme S1). The P3HT macroreagent was prepared through an externally-initiated polymerization reaction, which provided a higher degree of end-group functionality compared with conventional methods²³. The catalyst contained a tosylate functionality, which was then converted to an azide in a single post-polymerization reaction step. The PEO-alkyne macroreagent was prepared through Steglich esterification of commercially available monomethoxy-poly(ethylene oxide) and hexynoic acid. The P3HT prepared for this study had a M_n of 13.3 kDa, as measured by NMR end-group analysis and multi-angle laser light scattering. The PEO block had a M_n of 7.1 kDa. The polydispersity of the final block copolymer was 1.24, as measured by gel-permeation chromatography (GPC). Full details on our synthetic procedure including ¹H NMR characterization data and GPC data are provided in the Supporting Information, Figure S1.

We next desired to combine P3HT-*b*-PEO and V_2O_5 so as to obtain an intimately mixed, flexible, and electroactive electrode. Inspired by earlier approaches^{16,18,24–27}, we first attempted *in situ* synthesis of V_2O_5 in the block copolymer as well as direct mixing of the two components in various solvents or as dry powders. However, none of these approaches yielded electrodes with appreciable electrochemical activity. This result might be explained by considering prior reports on polyaniline/ V_2O_5 hybrid electrodes, where it was observed that polyaniline reduced V^{5+} to V^{4+} and the overall electrochemical activity was reduced¹⁷. In comparison, it is possible that similar interactions between P3HT and V_2O_5 might have led to the observed negligible electrochemical activity.

An alternative water-based approach met with much greater success. First, P3HT-*b*-PEO and lithium bis(trifluoromethanesulfonyl)imide (LiTFSI) were dispersed in water using sonication. The molar ratio of Li^+ to ethylene oxide repeat units was kept at 0.085²⁸, which has been reported to be an optimal ratio for lithium-ion conduction²⁹. Although P3HT-*b*-PEO is insoluble in water, after 1 h sonication, a uniform dispersion was formed (Fig. 1a). The block copolymer dispersion was stable for up to a week, after which large aggregates precipitated. The dispersion itself was purple in color and transparent. Other groups have used mixed solvents or dialysis to disperse P3HT-*b*-PEO block copolymers in water^{30–32}, but our approach centers upon only sonication. From hereafter, hybrid electrodes containing x wt% polymer are called “Px”.

We propose that a micellization and aggregation process, in which hydrophilic PEO forms a corona around hydrophobic P3HT, is responsible for the dispersion's stability. In support of this, TEM images of the drop-cast dispersion revealed a micellar aggregate diameter of ~320 nm, Fig. 1b. The dark core (~200 nm diameter) is likely the hydrophobic P3HT block, and the lighter shell (~60 nm in thickness) is likely the hydrophilic PEO block. The exact structure of the micellar aggregate remains a topic of future study. Dynamic light scattering (DLS) of the dispersion yielded an average aggregate diameter 250 nm (Figure S2), consistent with TEM results.

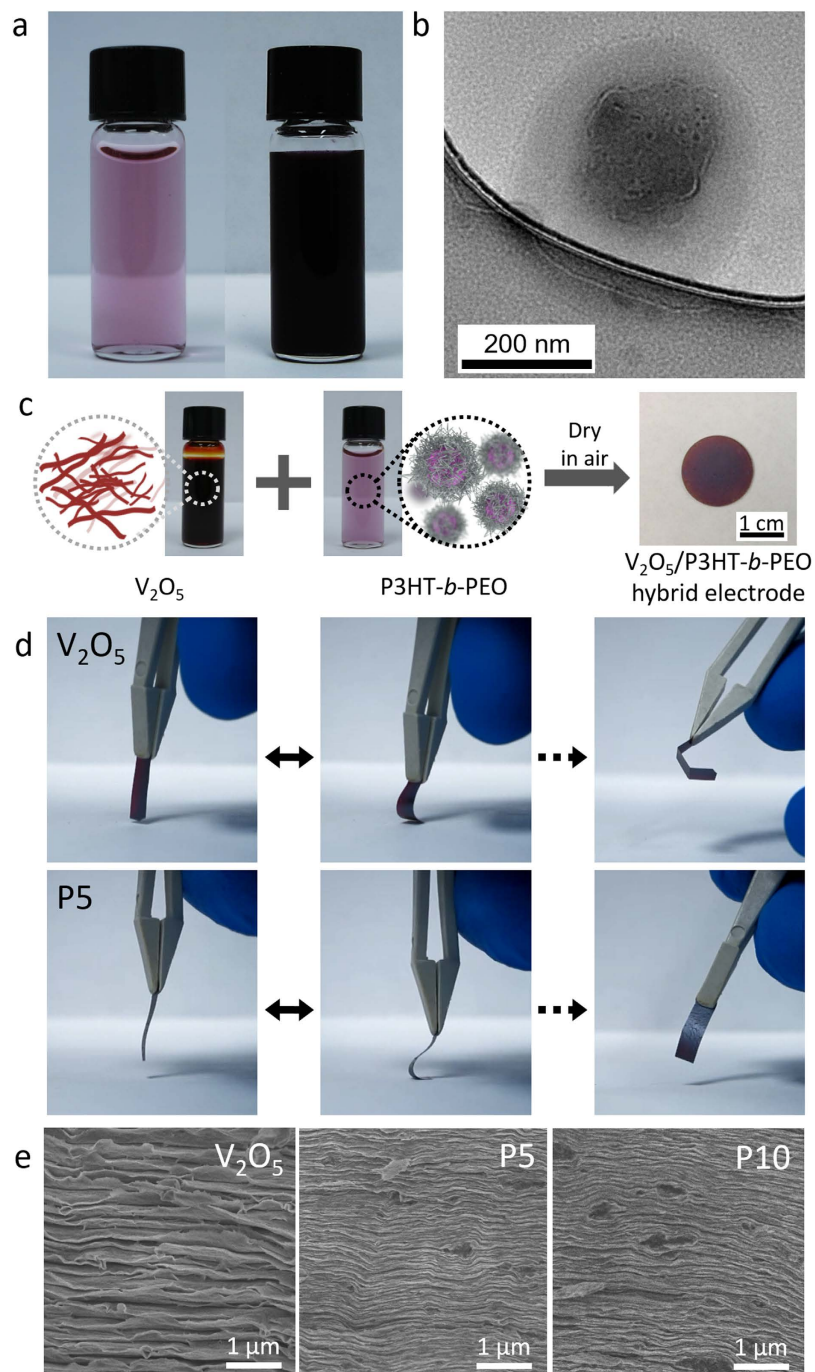


Figure 1. (a) P3HT-*b*-PEO dispersions at low concentration (0.05 mg/ml, left) and high concentration (1 mg/ml, right) with LiTFSI (the molar ratio of Li^+ to PEO repeat units was 0.085) in water, (b) transmission electron micrograph of a drop-cast P3HT-*b*-PEO micellar aggregate. (c) Schematic of P3HT-*b*-PEO/ V_2O_5 /LiTFSI cathode preparation (drawn by H.A.). (d) Digital images of a V_2O_5 /LiTFSI cathode (V_2O_5) (24 μm thick) and P5 (36 μm thick) in flexure. Movies are also provided in the Supporting Information. (e) Cross-sectional SEM images of V_2O_5 , P5, and P10 cathodes after failure during dynamic mechanical analysis. Micellar aggregates (black dots) were arranged between V_2O_5 layers in hybrid electrodes.

Having successfully made the P3HT-*b*-PEO dispersion, it was next mixed with aqueous V_2O_5 xerogel and sonicated, Fig. 1c. The mixture was then drop-cast, air-dried, and annealed at 90 °C. We prepared cathodes with total polymer content ranging from 1–50 wt % to assess the effect of block copolymer content on mechanical and electrochemical properties. Whereas neat V_2O_5 cathodes were brittle and failed under modest flexure, all hybrid cathodes were found to be flexible, (Fig. 1d, S3, Movies S1–S3).

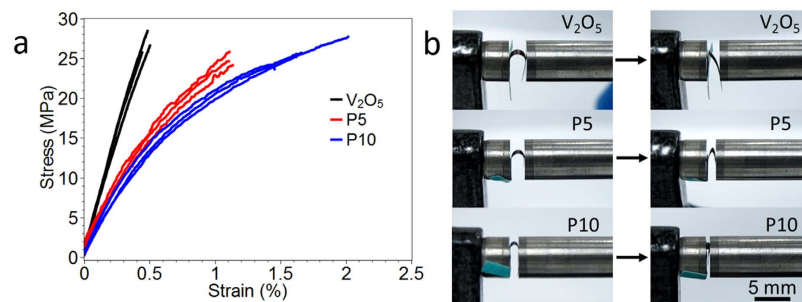


Figure 2. (a) Representative tensile profiles of hybrid electrodes in dependence of P3HT-*b*-PEO content and (b) digital images of collapsing radius test of hybrid electrodes. The collapsing radii of V₂O₅, P5, and P10 are 1.70, 0.40, and 0.30 mm, respectively. (Thickness of V₂O₅, P5, and P10: 26.9, 26.0, and 33.3 μm, respectively).

Sample	Tensile strength ^a σ (MPa)	Ultimate strain ^a ϵ (m/m)	Normal strain ^b $ \epsilon_x $ (m/m)	Young's modulus ^a E (GPa)	Toughness ^a W (kJ/m ³)
V ₂ O ₅	27 ± 2	0.0048 ± 0.0004	0.008 ± 0.003	6.0 ± 0.7	70 ± 8
P5	25 ± 1	0.011 ± 0.002	0.034 ± 0.13	3.7 ± 0.9	171 ± 5
P10	26 ± 2	0.017 ± 0.003	0.056 ± 0.006	3.5 ± 0.3	293 ± 73
PVdF10 ^c	24.1 ± 0.3	0.0078 ± 0.0006	0.010 ± 0.001	2.9 ± 0.6	99 ± 9

Table 1. Mechanical properties of hybrid electrodes derived from the stress-strain curves under tensile loading^a and from the collapsing radius test^b respectively. ^aValues obtained are an average of three samples for each tensile test. ^bValues obtained are an average of three samples for each collapsing radius experiment. ^cPVdF10 consists of 10 wt% PVdF and 90 wt% V₂O₅.

Cross-sectional SEM images reveal the fractured edges of neat V₂O₅, P5, and P10 cathodes. Well-packed V₂O₅ layers were visible throughout, Fig. 1e. The dark regions observed for P5 and P10 hybrid electrodes are likely micellar aggregates sandwiched between layers or locations at which aggregates had been pulled out during the fracturing process. SEM of the surface reveals a rough but uniform morphology, indicating that there is no large-scale phase separation (Figure S4). AFM images of the V₂O₅ and P5 cathode surfaces showed some evidence of micellar aggregates on the P5 electrode's surface, Figure S5.

The microstructure of the P3HT-*b*-PEO/LiTFSI/V₂O₅ cathodes was analyzed using grazing-incidence wide-angle X-ray scattering (GIWAXS). Films for GIWAXS analysis were prepared by drop-casting onto glass slides followed by air-drying and vacuum annealing at 70 °C, similar to the procedure used for cathode preparation. As shown in Figure S6, P3HT-*b*-PEO/LiTFSI/V₂O₅ films exhibited wide-angle scattering peaks at $q = 0.38 \text{ \AA}^{-1}$ and 0.64 \AA^{-1} , corresponding to primary scattering peaks for regioregular P3HT³³ and V₂O₅·*n*H₂O xerogels⁵, respectively. The most intense peak at 0.64 \AA^{-1} corresponds to quasi-ordered V₂O₅·*n*H₂O³⁴. An additional peak at 1.70 \AA^{-1} was also apparent from linecut analysis along the q_z direction, corresponding to the (003) plane of V₂O₅·*n*H₂O⁵. Peaks at 0.38, 0.8, and 1.2 \AA^{-1} correspond to regioregular P3HT crystallization in the edge-on orientation. An in-plane peak at $q_y = 1.66 \text{ \AA}^{-1}$ was evident by linecut analysis and corresponds to face-to-face π - π stacking of P3HT chains.

These measurements reveal crystallization of P3HT and V₂O₅·*n*H₂O in the composite cathodes. Scattering peaks match those for pure P3HT and V₂O₅·*n*H₂O, suggesting phase segregation and crystallization of each component within discrete domains. Additionally, crystallites for P3HT and V₂O₅·*n*H₂O are oriented in the out-of-plane direction, as commonly observed for thermally annealed thin films³³. Differential scanning calorimetry revealed only a P3HT crystallization peak (Figure S7), which suggests phase segregation and crystallization of P3HT blocks but not of PEO, consistent with the GIWAXS. This indicates that PEO crystallization was restricted since polymer chains were intercalated into V₂O₅ layers.

We next sought to quantify the mechanical properties using tensile testing and collapsing radius experiments. Figure 2a shows stress-strain curves for V₂O₅, P5, and P10 electrodes in triplicate, and Table 1 summarizes the average and standard deviation values of tensile strength, ultimate strain, Young's modulus, and toughness (see also Table S1). Both V₂O₅ and hybrid electrodes exhibited tensile behavior very similar to that of graphene oxide paper, in which three regimes (straightening, elastic, and plastic) successively occur during elongation. P10 exhibited the highest ultimate strain and toughness, whereas the Young's modulus decreased and the tensile strength remained unchanged. It is noteworthy that only 10 wt% polymer (P10) is required to obtain a 320% increase in toughness and a 250% increase in ultimate strain relative to polymer-free V₂O₅; this enhancement in mechanical properties does not come at the cost of tensile strength, but does cause a decrease in Young's modulus. SEM images suggest that the

enhanced ultimate strain and toughness enhancements come from well-dispersed P3HT-*b*-PEO micelles between V₂O₅ slabs, improving the flexibility of hybrid electrodes, Fig. 1e.

The mechanical properties of the hybrid electrodes are comparable, and in some cases higher, than that of graphene oxide paper and carbon nanotube sheets. For example the tensile strength of the P10 electrode was about four times higher than that of single-walled carbon nanotube Bucky paper (6.3 MPa), whereas the Young's modulus was only slightly higher (3.5 vs. 2.3 GPa, respectively)³⁵. In comparison, P10's tensile strength and modulus was 66% and 16% that of graphene oxide paper of similar thickness (22–25 μm, average values of 39 MPa and 22 GPa, respectively). Notably, P10's toughness was within range of that of graphene oxide paper (293 vs. 251 kJ/m³, respectively)¹⁰. On the other hand, the ultimate strain of P10 was far greater than that of graphene oxide paper (5.6% vs. 0.31%, respectively)^{10,36}. These results show that the similarities in the mechanical properties between V₂O₅ hybrid electrodes, Bucky paper, and graphene oxide paper, which are largely attributed to the interlocking nature of the nanomaterials, similar to the morphology shown in Fig. 1e. A comparison with poly(vinylidene difluoride) (PVdF, Table 1) binder shows no remarkable improvement relative to P10, which suggests that the unique block copolymer structure is responsible for the enhanced mechanical properties.

Bending experiments were also conducted with hybrid electrodes, Fig. 2b, Table 1, and Table S2. A strip of a hybrid electrode with thickness d_{film} was bent so that a simple curve was formed and then compressed between two parallel plates, Figure S8. The radius of curvature R_{col} was taken at the first sign of kink formation. The normal strain ε_x at the surface was calculated by $|\varepsilon_x| = 0.5d_{film}/R_{col}$ ³⁷. The images in Fig. 2b clearly show that the samples sustained a greater collapsing radius as polymer content increased. This enhancement is attributed to the polymer, which acts as a glue, holding the V₂O₅ sheets together. Here too, PVdF binder showed no remarkable enhancement relative to P10. This result emphasizes that the P3HT-*b*-PEO polymer and the self-assembled structure is superior to conventional fluoropolymer binders in terms of mechanical performance.

We next turn to the electrochemical properties of hybrid electrodes. Both V₂O₅ and P3HT are capable of storing energy, but V₂O₅ is expected to dominate charge storage behavior because P3HT has a near-negligible capacity (less than 10 mAh/g)^{20,21}. We found that for up to 50 wt% P3HT-*b*-PEO, the electrode showed no signs of dissolution into the electrolyte. However at higher polymer content, the electrolyte turned purple, suggestive of some amount of P3HT-*b*-PEO dissolution, Figure S9. Therefore, we investigated only hybrid electrodes containing up to 15 wt% polymer. At and above this concentration, the electrochemical performance was very poor, which we attribute to the low V₂O₅ content. A half-cell was assembled, and the hybrid electrode was used as the cathode, lithium foil as the anode, and 1 M LiTFSI in propylene carbonate as the electrolyte. Typical electrode thicknesses were in the range of 1.5 to 5 μm.

Cyclic voltammetry of the P3HT-*b*-PEO/V₂O₅/Li half-cell was carried out in the range of 2–3.8 V vs. Li/Li⁺ at a scan rate 0.1 mV/s for various polymer loadings, Fig. 3a. For V₂O₅, two distinct redox peaks appear at around 3.0 and 2.5 V in the cathodic/anodic scans consistent with insertions at a- and b-sites^{26,38,39}. For compositions above 10 wt% P3HT-*b*-PEO, the current decreased significantly, suggesting diminished electrochemical activity. For V₂O₅ alone (Fig. 3b), as the scan rate increased, the V₂O₅ voltammogram became distorted, obscuring the higher voltage peak. On the other hand for P10 (Fig. 3c), little distortion was observed, suggestive of reduced Ohmic overpotential and increased accessibility of lithium ions into the xerogel⁴⁰. The P3HT redox peak was observed only at very high polymer loadings; in Figure S10, P50 exhibited a small P3HT redox peak at 3.3 V²¹.

Figure 3d shows five galvanostatic charge-discharge cycles for P3HT-*b*-PEO/V₂O₅ hybrid electrodes of various compositions at a discharge rate of 0.1 C. From 3.8 to 2.0 V, a sloping discharge profile was obtained, typical of V₂O₅ xerogels^{41–45}. The b-site Li⁺ intercalation reaction (at ~2.5 V) was also observed during cycling. V₂O₅ alone exhibited an average discharge capacity and Coulombic efficiency of 220.9 mAh g⁻¹ and 99.4%, respectively. As the polymer content increased, the capacity decreased (P5: 193.3 mAh g⁻¹ and P10: 187.2 mAh g⁻¹) and the Coulombic efficiency decreased only slightly (P5: 99.5% and P10: 98.8%). The P5 electrode exhibited only a slight decrease in capacity relative to the pure V₂O₅ electrode, whereas the P15 exhibited a much larger decrease (100.2 mAh g⁻¹). We also examined a thicker P10 electrode, where it was found that capacity dropped from 187.2 mAh g⁻¹ to 40 mAh g⁻¹ (5 μm vs. 50 μm, respectively), which we attribute to diffusion limitations in thicker electrodes. The derivative of the galvanostatic cycle was taken with respect to voltage to obtain the incremental capacity, Fig. 3e. The peaks displayed were similar to those observed in cyclic voltammograms. Cycling was also conducted at various C-rates, in which a drop in capacity with increasing C-rate was observed, Fig. 3f. From electrochemical impedance spectroscopy at 2.6 V vs. Li/Li⁺, where V₂O₅ is particularly active, the diffusion coefficients (D_{Li^+}) were calculated for V₂O₅, P5, and P10 cathodes^{46–48}, Figure S11. The diffusion coefficient increased with polymer content, suggesting that lithium ion diffusion was enhanced by the P3HT-*b*-PEO diblock copolymer (D_{Li^+} of V₂O₅, P5 and P10: 0.85×10^{-11} , 1.64×10^{-11} , and 2.09×10^{-11} cm²/s, respectively). A full study of the charge storage mechanism as a function of polymer content is underway.

To demonstrate the union of good mechanical properties with energy storage, we constructed a prototype flexible half-cell, Fig. 3h,i. The flexible battery was assembled with lithium ribbon as the anode and a P5 hybrid electrode as the cathode. Celgard film and 1 M LiTFSI in propylene carbonate were used as the separator film and electrolyte. Polydimethylsiloxane film with 1 mm thickness was used as packaging.

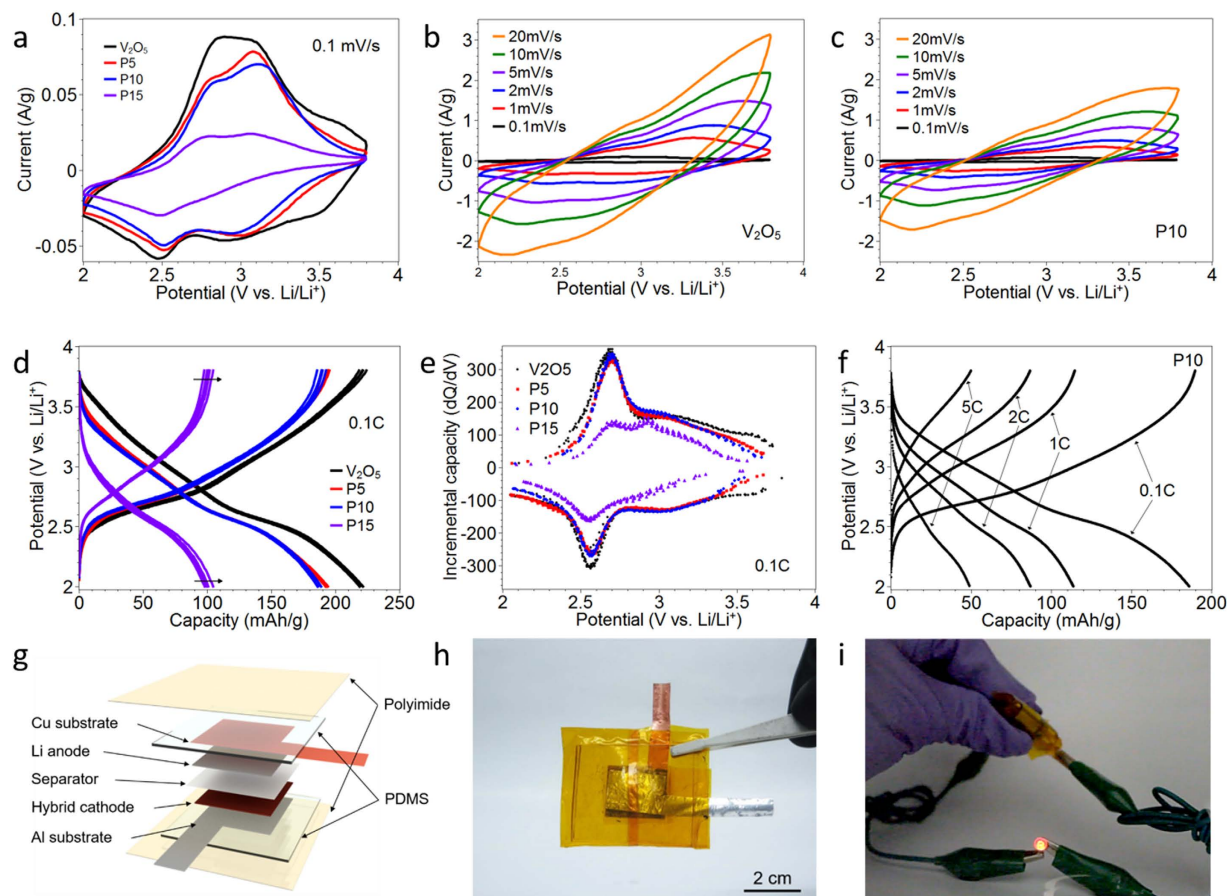


Figure 3. Cyclic voltammograms of (a) all compositions at 0.1 mV/sec, (b) V_2O_5 at various scan rates, and (c) P10 at various scan rates. All samples were approximately $4\mu\text{m}$ in thickness. (d) Charge-discharge behavior of V_2O_5 , P5, P10, and P15 electrodes at 0.1 C-rate and (e) incremental capacity (dQ/dV) taken from Fig. 3d. (f) Charge-discharge behavior at varying C-rates (0.1 to 5C) for a P10 cathode. For panels a–f, data were obtained from a two-electrode half-cell with lithium metal anode and 1 M LiTFSI in propylene carbonate. The capacity is based on mass of V_2O_5 . (g) A schematic illustration of the assembled flexible half-cell using the P5 hybrid cathode and digital images of (h) the flexible battery as-assembled. (i) The flexible half-cell lights an LED while bending (also see Movie S4).

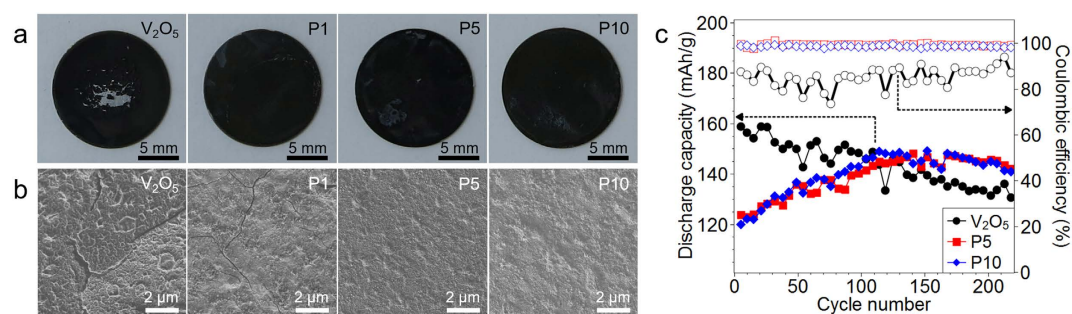


Figure 4. (a) Digital images of hybrid electrodes and (b) SEM images of hybrid electrodes after CV test. (c) Cycling behavior of V_2O_5 , P5, and P10 electrodes at a discharge rate of 1C.

To seal the cell more firmly, a polyimide film was used. The battery was repeatedly bent and flexed, and the LED light maintained its illumination, Fig. 3i and Movie S4.

V_2O_5 is very sensitive to cycling, in which changes in volume have led to reduced cycle life and irreversible damage to the electrode. Post-mortem SEM analysis of our electrodes after cycling illustrate cracks, and digital images show large-scale flaking of the electrode, Fig. 4a,b and Figure S12. However

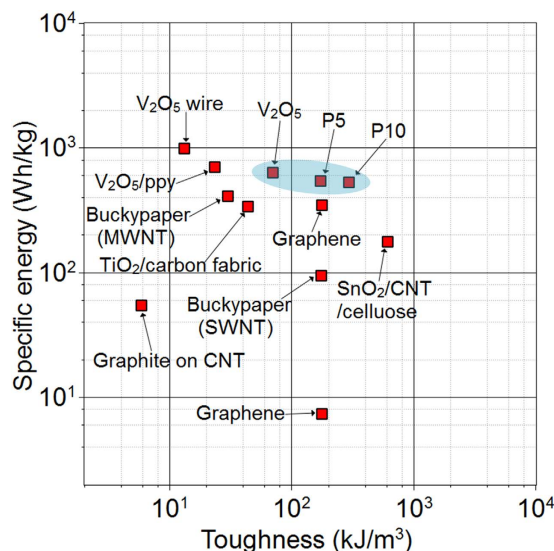


Figure 5. An Ashby plot of specific energy vs. toughness. Specific energy is reported as per mass of electrode. Data are taken from literature, discussed in main text, and data presented herein.

with just 5 wt% polymer, the formation of cracks and flakes appears to be completely arrested. Accelerated cycling (Fig. 4c, Figure S13-S14) demonstrates a gradual capacity fade for V_2O_5 , but P5 and P10 do not. Instead, the capacity of P5 and P10 gradually increases as electrolyte penetrates into the film with each cycle. After 100 cycles, the discharge capacity P5 and P10 electrodes exceeds that of V_2O_5 . Furthermore, the Coulombic efficiency is enhanced for the P5 and P10 electrodes. These results demonstrate that the polymer acts as a good binder, and only a small amount is required to achieve good cyclability.

Figure 5 shows an Ashby plot of specific energy vs. toughness, summarizing data from the literature and data presented here. Since our focus in this study is the electrode, we present electromechanical properties for the electrode alone. Our electrodes show a good combination of both mechanical and electrochemical properties as compared to Buckypaper (SWNT^{5,6} and MWNT^{7,8}), reduced graphene oxide paper^{9,10,12}, graphite on super-aligned CNTs¹², TiO_2 on activated carbon fabric¹², V_2O_5 wires¹³ and polypyrrole (ppy)-coated V_2O_5 wires¹³, Table S3. In the context of structural energy, it is important to note that one desires to maximize both mechanical and electrochemical properties. From the results, it is clear that it is very difficult to get both exceptional mechanical properties and electrochemical performance in one single electrode. One property often comes at the cost of another. One example of this here is with polymer content, in which increasing the polymer content enhances mechanical properties at the cost of capacity or energy. Still, for applications where both properties are desired it is more practical to find an electrode that marries the two even if there exists a trade-off.

Conclusions

This paper outlines a simple, water-based route to self-assemble diblock copolymers bearing electron- and ion-conducting blocks with V_2O_5 to form a flexible hybrid battery cathode. Only a small amount of the diblock copolymer is required to realize significant gains in mechanical properties without significantly sacrificing electrochemical properties. Further, this polymer halted the progression of mechanical failure, a common problem for V_2O_5 electrodes, which suffer from severe volume expansion. In the context of structural energy and power, in which one must balance mechanical with electrochemical properties, these electrodes are particularly interesting. They are far more flexible than V_2O_5 alone, and they exhibit mechanical properties comparable with that of Bucky paper and reduced graphene oxide paper. Our future work will detail the morphology and structure of the electrode, along with a detailed analysis of charge storage mechanisms.

Methods

Materials. Vanadium pentoxide, lithium bis(trifluoromethanesulfonyl)imide (LiTFSI), poly(vinylidene fluoride) (PVdF, molecular weight = 534,000 g/mol), N-methyl-2-pyrrolidone (NMP), and propylene carbonate (PC) were purchased from Sigma Aldrich. Lithium ribbon was purchased from Alfa Aesar. All chemicals were used as received. 316 stainless steel coins used as substrates were purchased from MTI Corporation. Water was purified to $18.2 M\Omega\text{-cm}$ (Milli-Q, Millipore). PEO-OH was purchased from Aldrich (lot# BCBB1016, 7.17 kg mol^{-1} by $^1\text{H NMR}$).

Synthesis of V_2O_5 xerogel and $P_3\text{HT-}b\text{-PEO}$ block copolymer. Described in the Supplementary Information.

Preparation of polymer suspensions. A VWR Symphony ultrasonic cleaner (VWR Model 97043-936, 35 kHz) was used to prepare the polymer dispersion. P3HT-*b*-PEO suspensions were made by sonicating the polymer and LiTFSI in Milli-Q water at 0 °C to make a 4 mg/mL stock solution. The molar ratio of ethylene oxide units to lithium ions was 0.085. Before making composites, aliquots of 4 mg/mL P3HT-*b*-PEO solutions were diluted to 1 mg/mL. Hydrodynamic diameter was determined using dynamic light scattering (DLS) (ZetasizerNano ZS90, Malvern) at 25 °C. For DLS, the P3HT-*b*-PEO solution was diluted to 0.05 mg/mL.

Cathode preparation. Before use, 316 stainless steel coins (12 mm diameter × 1.6 mm thickness) were cleansed *via* sonication for 15 minutes each in dichloromethane, acetone, water, and isopropanol, followed by drying under vacuum overnight at room temperature. Composites were made by mixing together appropriate volumes of 1 mg/mL P3HT-*b*-PEO (diluted from 4 mg/mL solutions) and 16.7 mg/mL V₂O₅ xerogel solutions in Milli-Q water. These solutions were drop-cast on stainless steel coins by depositing 0.97–1.12 mg worth of material (polymer + V₂O₅) onto the surface. Hereafter, electrodes containing X wt% polymers will be called “PX”. After drying in air, the cathodes were held under vacuum at 90 °C for 16 hours. For the electrodes containing PVdF, these were prepared by mixing V₂O₅ with PVdF in NMP. The mixture was cast as before and allowed to dry at 70 °C for three hours, and then 90 °C overnight under vacuum.

Cathode morphologies were investigated using scanning electron microscopy (SEM, JEOL JSM-7500F). Grazing incidence wide angle x-ray scattering measurements were carried out on Sector 8-ID-E at Advanced Photon Source, Argonne National Laboratory⁴⁹. Beamline 8-ID-E operates at an energy of 7.35 keV and images were collected from a Pilatus 1MF camera (Dectris), with two exposures for different vertical position of the detector. After flatfield correction for detector nonuniformity, the images are combined to fill in the gaps for rows at the borders between modules, leaving dark only the columns of inactive pixels at the center. Using the GIXSGUI package⁵⁰ for Matlab (Mathworks), data are corrected for x-ray polarization, detector sensitivity and geometrical solid-angle. The beam size is 200 μm (h) × 20 μm (v). Sample detector distance is 204 mm. Sample measurement and thermal annealing were carried out under vacuum which is in the range of 2–3 × 10⁻⁶ bar, with the sample stage interfaced with a Lakeshore 340 unit.

Cell assembly and measurement. Electrochemical measurements were performed in two electrode cells (Tomcell Japan Co., Ltd.) assembled in a water-free, oxygen-free, argon-filled glovebox (MBraun) using lithium metal anodes. 1.0 M LiTFSI in propylene carbonate was used as the electrolyte and Celgard 3501 was used as the separator. Cyclic voltammetry, galvanostatic measurements, and impedance spectroscopy were performed using a Gamry Interface 1000, Solartron SI 1287, and Solartron 1470E.

Free-standing film preparation and mechanical testing. P3HT-*b*-PEO/V₂O₅ mixtures were cast onto polystyrene weigh-boats (VWR), followed by air-drying. Following isolation from the weigh-boat, the hybrid electrodes were cut into rectangular strips of approximately 1 mm × 18 mm for testing. Static mechanical tensile tests were performed using a dynamic mechanical analyzer (DMA-Q800, TA Instruments). All tensile tests were conducted in controlled-force mode with a strain rate of 0.2%/min and preload of 0.02 N.

References

- Nyholm, L., Nyström, G., Mhrihanyan, A. & Strømme, M. Toward flexible polymer and paper-based energy storage devices. *Advanced Materials* **23**, 3751–3769, doi: 10.1002/adma.201004134 (2011).
- Ling, Z. *et al.* Flexible and conductive MXene films and nanocomposites with high capacitance. *Proceedings of the National Academy of Sciences* **111**, 16676–16681 (2014).
- Shirshova, N. *et al.* Multifunctional structural energy storage composite supercapacitors. *Faraday discussions* **172**, 81–103 (2014).
- Snyder, J. F., Carter, R. H. & Wetzel, E. D. Electrochemical and mechanical behavior in mechanically robust solid polymer electrolytes for use in multifunctional structural batteries. *Chemistry of materials* **19**, 3793–3801 (2007).
- Ng, S. *et al.* Single wall carbon nanotube paper as anode for lithium-ion battery. *Electrochimica Acta* **51**, 23–28 (2005).
- Whitten, P. G., Spinks, G. M. & Wallace, G. G. Mechanical properties of carbon nanotube paper in ionic liquid and aqueous electrolytes. *Carbon* **43**, 1891–1896 (2005).
- Lee, S. W. *et al.* High-power lithium batteries from functionalized carbon-nanotube electrodes. *Nature Nanotechnology* **5**, 531–537 (2010).
- Riguer, J. L., Hasan, S. A., Mahajan, S. V. & Dickerson, J. H. Buckypaper fabrication by liberation of electrophoretically deposited carbon nanotubes. *Carbon* **48**, 4090–4099 (2010).
- Yang, X., Zhu, J., Qiu, L. & Li, D. Bioinspired effective prevention of restacking in multilayered graphene films: towards the next generation of high-performance supercapacitors. *Advanced Materials* **23**, 2833–2838 (2011).
- Dikin, D. A. *et al.* Preparation and characterization of graphene oxide paper. *Nature* **448**, 457–460 (2007).
- Wang, K. *et al.* Super-aligned carbon nanotube films as current collectors for lightweight and flexible lithium ion batteries. *Advanced Functional Materials* **23**, 846–853 (2013).
- Liu, S. *et al.* A flexible TiO₂(B)-based battery electrode with superior power rate and ultralong cycle life. *Advanced Materials* **25**, 3462–3467 (2013).
- Noerochim, L. *et al.* Impact of mechanical bending on the electrochemical performance of bendable lithium batteries with paper-like free-standing V₂O₅-polypyrrole cathodes. *Journal of Materials Chemistry* **22**, 11159–11165 (2012).
- Wang, Y., Takahashi, K., Lee, K. H. & Cao, G. Z. Nanostructured vanadium oxide electrodes for enhanced lithium-ion intercalation. *Advanced Functional Materials* **16**, 1133–1144, doi: 10.1002/adfm.200500662 (2006).
- Zhang, C., Chen, Z., Guo, Z. & Lou, X. W. D. Additive-free synthesis of 3D porous V₂O₅ hierarchical microspheres with enhanced lithium storage properties. *Energy Environ. Sci.* **6**, 974–978 (2013).

16. Goward, G., Leroux, F. & Nazar, L. Poly(pyrrole) and poly(thiophene)/vanadium oxide interleaved nanocomposites: positive electrodes for lithium batteries. *Electrochimica acta* **43**, 1307–1313 (1998).
17. Leroux, F., Goward, G., Power, W. P. & Nazar, L. F. Electrochemical Li insertion into conductive polymer/ V_2O_5 nanocomposites. *Journal of The Electrochemical Society* **144**, 3886–3895, doi: 10.1149/1.1838107 (1997).
18. Olivetti, E. A., Kim, J. H., Sadoway, D. R., Asatekin, A. & Mayes, A. M. Sol-gel synthesis of vanadium oxide within a block copolymer matrix. *Chemistry of Materials* **18**, 2828–2833, doi: 10.1021/cm060119s (2006).
19. Bates, F. S. & Fredrickson, G. H. Block copolymer thermodynamics: theory and experiment. *Annual Review of Physical Chemistry* **41**, 525–557 (1990).
20. Javier, A. E., Patel, S. N., Hallinan, D. T., Srinivasan, V. & Balsara, N. P. Simultaneous electronic and ionic conduction in a block copolymer: application in lithium battery electrodes. *Angewandte Chemie International Edition* **50**, 9848–9851, doi: 10.1002/anie.201102953 (2011).
21. Patel, S. N., Javier, A. E. & Balsara, N. P. Electrochemically oxidized electronic and ionic conducting nanostructured block copolymers for lithium battery electrodes. *ACS Nano* **7**, 6056–6068, doi: 10.1021/nn4018685 (2013).
22. Kempf, C. N., Smith, K. A., Pesek, S. L., Li, X. & Verduzco, R. Amphiphilic poly(alkylthiophene) block copolymers prepared via externally initiated GRIM and click coupling. *Polymer Chemistry* **4**, 2158–2163, doi: 10.1039/C3PY21098G (2013).
23. Bronstein, H. A. & Luscombe, C. K. Externally initiated regioregular P3HT with controlled molecular weight and narrow polydispersity. *Journal of the American Chemical Society* **131**, 12894–12895, doi: 10.1021/ja9054977 (2009).
24. Huguenin, F., Giz, M. J., Ticianelli, E. A. & Torresi, R. M. Structure and properties of a nanocomposite formed by vanadium pentoxide containing poly (*N*-propane sulfonic acid aniline). *Journal of power sources* **103**, 113–119 (2001).
25. Lira-Cantú, M. & Gómez-Romero, P. The organic-inorganic polyaniline/ V_2O_5 system. application as a high-capacity hybrid cathode for rechargeable lithium batteries. *Journal of The Electrochemical Society* **146**, 2029–2033 (1999).
26. Park, N.-G. *et al.* Synthesis and electrochemical properties of V_2O_5 intercalated with binary polymers. *Journal of Power Sources* **103**, 273–279, doi: 10.1016/S0378-7753(01)00863-1 (2002).
27. Wong, H. Synthesis and characterization of polypyrrole/vanadium pentoxide nanocomposite aerogels. *Journal of Materials Chemistry* **8**, 1019–1027 (1998).
28. Wanakule, N. S. *et al.* Ionic conductivity of block copolymer electrolytes in the vicinity of order-disorder and order-order transitions. *Macromolecules* **42**, 5642–5651 (2009).
29. Patel, S. N., Javier, A. E., Stone, G. M., Mullin, S. A. & Balsara, N. P. Simultaneous conduction of electronic charge and lithium ions in block copolymers. *ACS Nano* **6**, 1589–1600, doi: 10.1021/nn2045664 (2012).
30. Kamps, A. C., Fryd, M. & Park, S.-J. Hierarchical self-assembly of amphiphilic semiconducting polymers into isolated, bundled, and branched nanofibers. *ACS nano* **6**, 2844–2852 (2012).
31. Park, S.-J., Kang, S.-G., Fryd, M., Saven, J. G. & Park, S.-J. Highly tunable photoluminescent properties of amphiphilic conjugated block copolymers. *Journal of the American Chemical Society* **132**, 9931–9933 (2010).
32. Yang, H., Xia, H., Wang, G., Peng, J. & Qiu, F. Insights into poly(3-hexylthiophene)-*b*-poly(ethylene oxide) block copolymer: synthesis and solvent-induced structure formation in thin films. *Journal of Polymer Science Part A: Polymer Chemistry* **50**, 5060–5067 (2012).
33. Kline, R. J. *et al.* Dependence of regioregular poly(3-hexylthiophene) film morphology and field-effect mobility on molecular weight. *Macromolecules* **38**, 3312–3319 (2005).
34. Petkov, V. *et al.* Structure of $V_2O_5 \cdot nH_2O$ xerogel solved by the atomic pair distribution function technique. *Journal of the American Chemical Society* **124**, 10157–10162 (2002).
35. Coleman, J. N. *et al.* Improving the mechanical properties of single-walled carbon nanotube sheets by intercalation of polymeric adhesives. *Applied Physics Letters* **82**, 1682–1684 (2003).
36. Park, S. *et al.* Graphene oxide papers modified by divalent ions-enhancing mechanical properties via chemical cross-linking. *ACS nano* **2**, 572–578 (2008).
37. Timoshenko, S., Goodier, J. & Abramson, H. N. Theory of elasticity. *Journal of Applied Mechanics* **37**, 888 (1970).
38. Hibino, M., Ugaji, M., Kishimoto, A. & Kudo, T. Preparation and lithium intercalation of a new vanadium oxide with a two-dimensional structure. *Solid State Ionics* **79**, 239–244 (1995).
39. Gallote, N. A., Camargo, M. N., Iost, R. M., Crespihlo, F. & Huguenin, F. Effects of self-assembled materials prepared from V_2O_5 for lithium ion electroinsertion. *Langmuir* **27**, 12209–12217 (2011).
40. Le, D., Passerini, S., Tipton, A., Owens, B. & Smyrl, W. Aerogels and xerogels of V_2O_5 as intercalation hosts. *Journal of The Electrochemical Society* **142**, L102–L103 (1995).
41. West, K., Zachau-Christiansen, B., Jacobsen, T. & Skaarup, S. Vanadium oxide xerogels as electrodes for lithium batteries. *Electrochimica acta* **38**, 1215–1220 (1993).
42. Giorgetti, M. *et al.* In situ X-Ray absorption spectroscopy characterization of V_2O_5 xerogel cathodes upon lithium intercalation. *Journal of the Electrochemical Society* **146**, 2387–2392 (1999).
43. Passerini, S. *et al.* XAS and electrochemical characterization of lithium intercalated V_2O_5 xerogels. *Solid State Ionics* **90**, 5–14 (1996).
44. Tipton, A., Passerini, S., Owens, B. & Smyrl, W. Performance of lithium/ V_2O_5 xerogel coin cells. *Journal of the Electrochemical Society* **143**, 3473–3477 (1996).
45. Sathiyaraj, M., Prakash, A., Ramesha, K., Tarascon, J. M. & Shukla, A. V_2O_5 -anchored carbon nanotubes for enhanced electrochemical energy storage. *Journal of the American Chemical Society* **133**, 16291–16299 (2011).
46. Yu, J. *et al.* A porous vanadium pentoxide nanomaterial as cathode material for rechargeable lithium batteries. *Electrochimica Acta* **89**, 292–299 (2013).
47. Levi, M., Lu, Z. & Aurbach, D. Li-insertion into thin monolithic V_2O_5 films electrodes characterized by a variety of electroanalytical techniques. *Journal of power sources* **97**, 482–485 (2001).
48. Navone, C., Baddour-Hadjean, R., Pereira-Ramos, J. & Salot, R. A kinetic study of electrochemical lithium insertion into oriented V_2O_5 thin films prepared by rf sputtering. *Electrochimica Acta* **53**, 3329–3336 (2008).
49. Jiang, Z. *et al.* The dedicated high-resolution grazing-incidence X-ray scattering beamline 8-ID-E at the Advanced Photon Source. *Journal of Synchrotron Radiation (International Union of Crystallography—IUCr)* **19**, 627–636, doi: 10.1107/S090949512022017 (2012).
50. Jiang, Z. GIXSGUI software. Available at: <https://www1.aps.anl.gov/Sector-8/8-ID/Operations-and-Schedules/Useful-Links/Sector-8-GIXSGUI>. (Accessed: 23th July 2015).

Acknowledgments

This work is supported in part by NSF Grant No. 1336716 (electrochemical properties), NSF Grant CBET-1336073 (polymer synthesis, processing, and characterization), AFOSR-YIP (FA9550-13-1-0147) (mechanical properties), and Kwangjeong Educational Foundation.

Author Contributions

H.A., J.L. and R.V. wrote the main manuscript text. H.A. made the graphics in Figure 1. H.A. and J.M. prepared and characterized the hybrid electrodes' mechanical and electrochemical properties. K.S., L.S., Y.H.L. and S.P. synthesized the polymer and characterized the hybrid electrode by GISAXS. All authors reviewed the manuscript.

Additional Information

Supplementary information accompanies this paper at <http://www.nature.com/srep>

Competing financial interests: The authors declare no competing financial interests.

How to cite this article: An, H. *et al.* Highly Flexible Self-Assembled V₂O₅ Cathodes Enabled by Conducting Diblock Copolymers. *Sci. Rep.* **5**, 14166; doi: 10.1038/srep14166 (2015).



This work is licensed under a Creative Commons Attribution 4.0 International License. The images or other third party material in this article are included in the article's Creative Commons license, unless indicated otherwise in the credit line; if the material is not included under the Creative Commons license, users will need to obtain permission from the license holder to reproduce the material. To view a copy of this license, visit <http://creativecommons.org/licenses/by/4.0/>